THE JOURNAL OF PHYSICAL CHEMISTRY C
A JOURNAL OF THE AMERICAN CHEMICAL SOCIETY

pubs.acs.org/JPCC

Article

Plasmonics-Enhanced UV Photocatalytic Water Purification

Ryan Brisbin, Jenny Zhou, Tiziana Bond, Lars Voss, Aaron J. Simon, Ryan Baxter, and Allan S.P. Chang*

Cite This: J. Phys. Chem. C 2021, 125, 9730−9735

Read Online

ACCESS | Metrics & More | Article Recommendations | Supporting Information

ABSTRACT: Titanium dioxide (TiO_2) is commonly used for photocatalytic decomposition of organic contaminants for the purpose of water purification. One promising method to enhance TiO_2 photocatalysis is the incorporation of surface plasmon resonance on its surface where photocatalytic reactions take place. Herein, a novel methodology using plasmonically tuned aluminum nanostructures to enhance the rate of photodecomposition of aqueous methyl orange is demonstrated. These nanostructures are tuned to the TiO_2 band gap in the UV regime and patterned on TiO_2-coated substrates using nanosphere lithography. Compared to a blank TiO_2 film, the plasmonics is found to enhance the initial TiO_2 photocatalytic rate by up to 10 times, and further enhancement is possible upon refinement of the plasmonic technology.

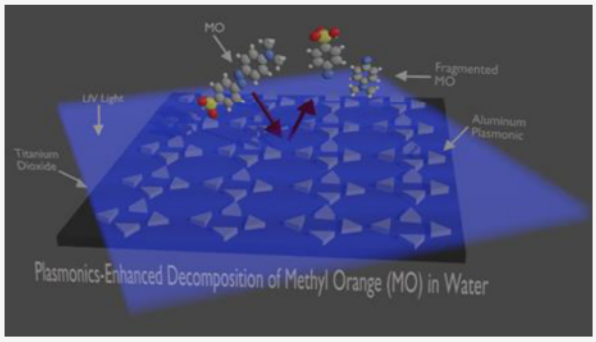

INTRODUCTION

Access to clean water is of critical importance to humanity, and increase in both industrialization and population has generated the need for less costly and faster methods of water purification of industrial contaminants.[1,2] The additive production in sectors of industry that necessitate the use of dyestuffs (textiles, paper mills, etc.) has led to an increase in the amount of colored wastewater.[3] Due to coloring being a principle indicator of (bad) water quality, new ways to either remove the dyes or decolor the water are paramount.[4] A primary component of most colored water waste streams is methyl orange (MO), an aromatic azo dye. Due to its prevalence in textile waste streams, the scientific community has adopted MO as a proxy for evaluating water purification systems using titanium dioxide as a photocatalyst. In order to maximize the amount of purification and minimize both the necessary components (excess reactants, costly materials, etc.), photocatalytic decomposition has been an area of significant investigation.

Photocatalysis using TiO_2 has seen a tremendous amount of development over the past 40 years.[5,6] The use of TiO_2 was pioneered in the early 1970s using a photoelectrochemical cell from the semiconducting material for the tandem photoelectrochemical splitting of water.[7] Following the advent of the initial discovery, the use of TiO_2 for photocatalytic redox processes expanded significantly due to its strong redox abilities, low cost, stability, and nontoxicity. Its use has also been expanded to broader applications such as sensing.[8−13] In particular, there is strong interest in application of TiO_2 in water purification.[14−17]

Through the continued progress in this area, the technology relying on the TiO_2 photocatalyst has been readily adapted for treatment of MO.[18−24] With the current successes of using TiO_2 to decompose MO, innovation is constantly sought out in order to improve upon the existing efficiency and reaction rates. Current approaches to improve the baseline catalytic activity of TiO_2 have been directed toward two primary routes: (1) additives, such as iron, tin, and carbon nanoparticles (np) and (2) nanostructures, such as carbon nanotubes or porous surfaces.[25−30]

Recently, there has been another approach to enhance photocatalysis through the combination of the photoexcitation of TiO_2 and surface plasmon.[31] The coupling of TiO_2 with surface plasmon, usually on gold, has shown the ability to enhance the redox capability and activity in systems using TiO_2.[11,32−35] While examples of this enhancement with gold are very prevalent in the literature, gold is effective only in the visible spectral range, where efficiency of TiO_2 photocatalysis is low. More recently, alternative plasmonic materials such as aluminum (Al) have been explored. Al is more cost-effective and can have UV plasmonic response that overlaps with the band gap of TiO_2.[36,37] Herein, a novel method using Al nanostructures for the purpose of increasing photo-activity and providing a catalytic rate enhancement in the decomposition process of MO through the activation of the Al surface plasmon is demonstrated. This system represents the first time this methodology has been used in a lithographically patterned substrate, which allows for precise tuning of the plasmonic response.

Received: January 23, 2021
Revised: April 4, 2021
Published: May 4, 2021

https://doi.org/10.1021/acs.jpcc.1c00613
J. Phys. Chem. C 2021, 125, 9730−9735

PLASMONICS SIMULATION

To guide the design of our Al nanostructures, 3D finite-element-method simulation was carried out using the commercial COMSOL program. Plane wave is incident upon an Al equilateral nanotriangle (which models the shape of the nanostructure patterned by our methodology as outlined below) sitting on top of a layer of TiO_2. An absorbing boundary condition was used. The geometry of the nanotriangle was varied to obtain resonance in the desired UV regime. This in turn guides our fabrication process parameters. For resonance at wavelength of 350 nm, which corresponds to the band edge of TiO_2, the side length of the equilateral nanotriangle is found to be 95 nm and thickness 30 nm. (Figure 1).

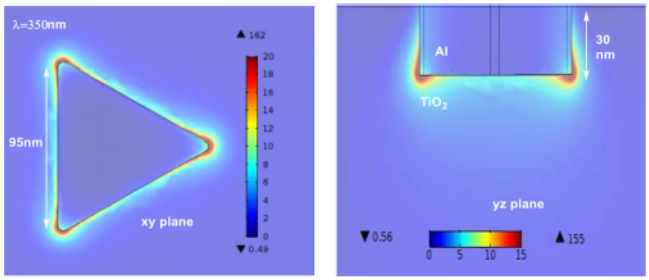

Figure 1. COMSOL simulation results showing the field enhancement of Al nanotriangle at photon energy above the TiO_2 band gap.

METHODS - CATALYST FABRICATION

The nanotriangles modeled by COMSOL were fabricated by nanosphere lithography. The five major steps in substrate fabrication are as follows: (1) TiO_2 film deposition, (2) self-assembly of polystyrene beads via spin-coating, (3) nanosphere tuning by plasma etching, (4) Al film deposition, and (5) lift-off. Fused silica wafers with thickness of 500 μm were used for substrate fabrication. The wafers were soaked in an 80 °C aqueous solution of deionized (DI) water, ammonia hydroxide, and hydrogen peroxide (5:1:1 volume ratio) for 30 min to remove any organic residues. This was followed by a thorough rinse with DI water and dried using nitrogen. Afterward, a 100 nm layer of TiO_2 was deposited by electron beam evaporation onto the wafer surface and further annealed at 500 °C for 1 hour in ambient air to obtain the TiO_2 anatase phase.[38,39] The catalytically active anatase phase was confirmed through X-ray diffraction (XRD) analysis shown in Figure 2 and compared to the reference pattern from JCPDS card no. 21−1272 for anatase TiO_2.[40,41] The confirmation of anatase was critical due to its higher photocatalytic activity compared to the rutile crystal structure.[42]

The wafers were cleaved into smaller substrates and cleaned in acetone and isopropyl alcohol and rinsed with DI water. Next, during nanosphere lithography, either 300 or 460 nm diameter polystyrene beads (Sigma Aldrich, St. Louis, MO) were spun onto the substrates using a commercial spin-coater, where the attractive forces of the beads lead to formation of a hexagonal-close packed monolayer (Figure 3A).[40,41,43−45] A total of three spin steps allow for (1) improved surface coverage, (2) monolayer generation, and (3) removal of nanospheres from edges. The three spin steps are as follows: (1) 1940 rpm for 10 s at a ramp rate of 308 rpm/sec, (2) 2300 rpm for 10 s at a ramp rate of 1001 rpm/sec, and (3) 6000 rpm for 15 s at a ramp rate of 1001 rpm/sec.

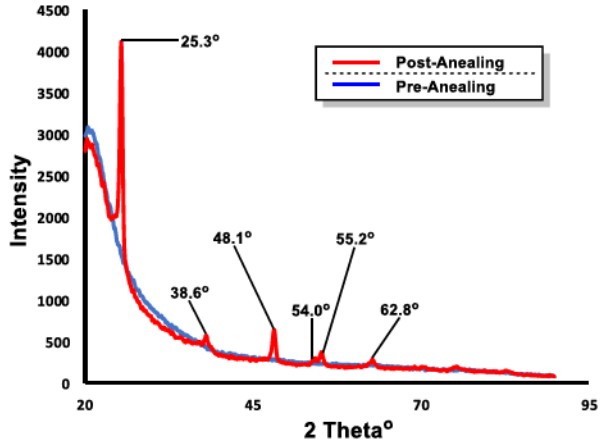

Figure 2. XRD patterns of the TiO_2 thin film before and after annealing at 500 °C. Peaks present after the anneal process refer to peaks specific to the anatase phase.

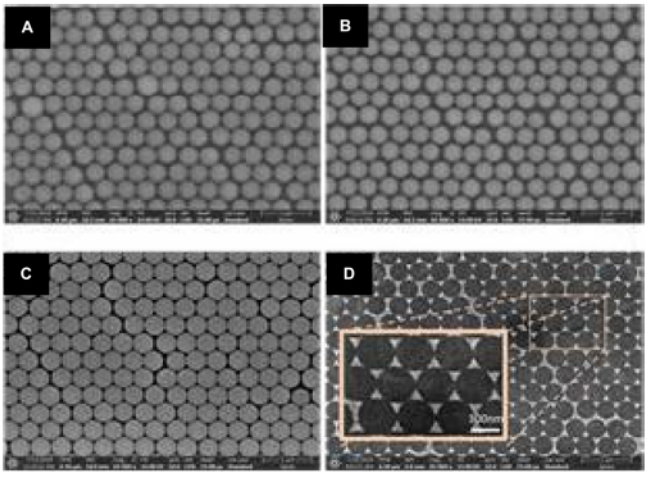

Figure 3. SEM images of the TiO_2 + Al plasmonic substrate microfabrication process. (3A) Monolayer of nanospheres on top of the anatase-phase TiO_2 film after nanosphere lithography. (3B) Plasma-etched nanospheres. (3C) E-beam deposition of Al on top of nanospheres. (3D) Post-nanosphere lift off in toluene.

The size of the polystyrene beads coated on the TiO_2 surface was tuned with plasma[36] to achieve the desired size using a parallel plate reactive ion etcher with a radio frequency power of 100 W and flow rate of 10 sccm O_2 and 36 sccm CF_4 for 75 s. (Figure 3B) Next, a 30 nm layer of Al was electron beam-deposited on top of the tuned polystyrene beads filling the gaps in between the beads. (Figure 3C) Finally, a majority of the beads were removed with tape, and the remaining beads were sonicated in toluene for 30 s to dissolve the polystyrene beads and remove the excess Al, leaving behind the Al patterns defined by the nanospheres on the TiO_2 surface. (Figure 3D).

After substrate manufacturing and tuning of the Al nanostructures, surface plasma resonance (SPR) activity was characterized via a UV−vis spectrophotometer (Perkin Elmer lambda 950) with an attached 60 mm integrating sphere. *An important note is that the size of polystyrene beads had a direct and significant effect on the Al feature size*, where the feature size refers to the side of the triangular Al pattern. The 300 nm polystyrene beads yield an average feature size of ≈ 90 nm,

https://doi.org/10.1021/acs.jpcc.1c00613
J. Phys. Chem. C 2021, 125, 9730−9735

while the 460 nm polystyrene beads yield average feature size of ≈ 120 nm. Along with change of Al feature size, red shifts were observed via increasing the size of the patterned Al nanostructures, with the 300 nm spheres yielding a higher degree of energy overlap between the Al nanostructure and TiO_2 thin film (Figure 4). The experimental absorptions of the

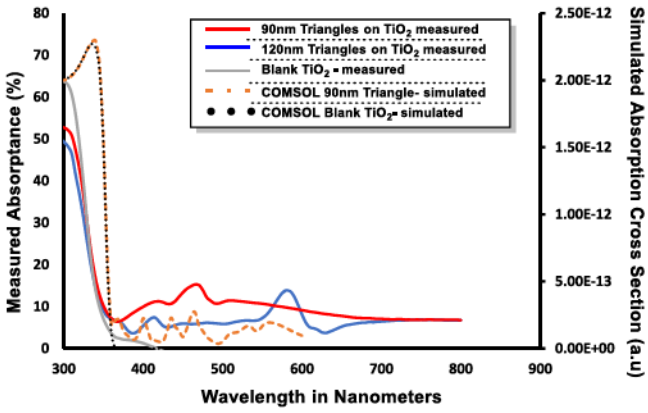

Figure 4. Measured UV−vis absorption of two Al structures of different sizes on TiO_2 90 nm triangles (red) and 120 nm triangles (blue). Also plotted are COMSOL simulated absorption cross section of 90 nm Al nanotriangles patterned on the TiO_2 thin film (dashed orange) and plain TiO_2 thin film (dotted black).

Al features were compared with COMSOL predicted absorptions of blank TiO_2 and a 90 nm Al triangle, in which similar absorptions are observed, as seen in Figure 4. The different feature sizes obtained by using two different sizes of polystyrene beads allowed for a deeper investigation into the effect of activation of the Al plasmon on catalysis.

METHYL ORANGE PLASMONICS-ENHANCED DECOMPOSITION

All reactions were conducted in a 6″ diameter boro-silicate petri dish and irradiated using an IntelliRay-600 UV shutter flood light set to 35% power with no temperature input. MO (1%W,V) was purchased from Sigma Aldrich. A Perkin Elmer lambda 950 UV−vis spectrophotometer with an attached 60 mm integrating sphere was used for all measurements for the following: (1) (pre-reaction) catalyst characterization, (2) MO concentration determination (via the MO absorption peak at 469 nm), and (3) post-reaction catalyst characterization. All experiments were conducted with a 15 mL aliquot of a batch solution with a 1:15 dilution of MO in DI water from the MO stock. Each time point was a self-contained and independent reaction using the same catalyst. (X time points = between 3−6 reactions).

All reactions were conducted on a 6 cm^2 substrate. The substrate was placed in a 6″ borosilicate petri dish and covered with 15 mL (measured via a volumetric flask) of dilute MO bulk solution. The substrate was equilibrated in solution for 10 mins, while the vessel was capped and wrapped in tin foil. The reaction vessel was placed in the UV flood light system and irradiated for incremental time periods. After exposure, solution was transferred into a clean and dry 15 mL volumetric flask and volume was restored to 15 mL to account for evaporative loss during the exposure, followed by inversion (4×). Following volume normalization and homogenization, a 1:100 dilution of the bulk sample was prepared in a plastic UV−vis cuvette for analysis, and the results were compared to a MO control spectrum to determine MO concentration loss (see supporting information).

Control reactions of MO with no catalyst system yielded negligible change in concentration through the entire exposure time. Both substrates (larger and smaller Al features) were tested for catalytic enhancement. The substrate with a larger Al nanotriangle feature size (≈ 120 nm) demonstrated a more red-shifted absorption spectra than the smaller feature size (≈ 90 nm) in the pre-reaction characterization. These off-tuned substrates showed a decrease in concentration over the 10-min irradiation period but was not significantly different from blank thin-film TiO_2 control experiment. The lack of plasmonic enhancement by the larger Al-feature sizes is believed to be caused by the lack of overlap between the Al plasmon and TiO_2.[46] Further refinement of the Al plasmonic feature by reducing the polystyrene nanospheres size to 300 nm effectively decreased the Al feature size from 120 to 90 nm, which increased the spectral overlap of the plasmonic Al nanostructure and TiO_2 (≈ 365 nm). As a result of the increase in spectral overlap, the 90 nm Al feature size yielded a significant rate enhancement over the course of the 10 min exposure, as demonstrated in Figure 5A.

The observed rate enhancement with the smaller Al nanofeatures was attributed to the successful transfer of energy from the localized SPR leading to enhanced photoexcitation of TiO_2. While the mechanism of energy transfer from the

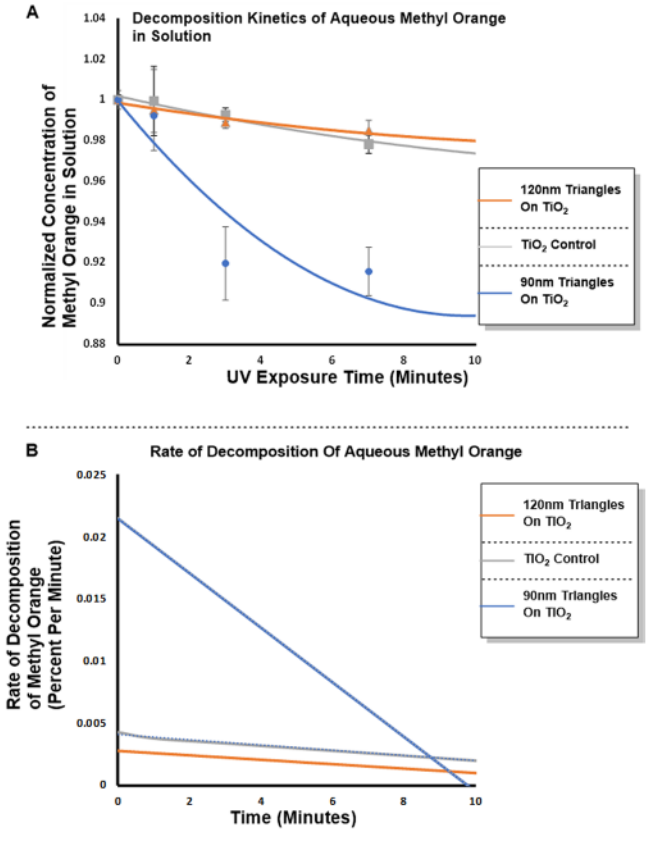

Figure 5. (A) Reaction kinetics plots of MO photodecomposition. Blank titanium dioxide thin-film control (gray), off-tuned Al nanostructure (orange), and tuned Al nanostructure (blue). (B) Plot of the first derivative of the measured MO concentration over time for all substrates.

https://doi.org/10.1021/acs.jpcc.1c00613
J. Phys. Chem. C 2021, 125, 9730−9735

activation of SPR to a semiconductor is still an area of active research, it is currently believed that the energy transfer between the Al surface plasmon and TiO_2 catalyst film occurs via two possible processes. A possible energy transfer mechanism is hot carrier injection through resonant energy transfer.[47,48] The discrepancy between the simulated and observed catalyst absorption spectra could be due to various variables that are currently not accounted for in the simulations (e.g., sample inhomogeneity, Al structure spacing, etc.). Due to this discrepancy between our simulations and observed data, another possible mechanism of the observed increased catalytic activity can be through a nonresonant route such as Landau damping effect and accompanied electron scattering.[47,49−51] This claim is rationalized through the higher absorption of 90 nm Al structures in the UV region compared to 120 nm Al structures. This system, however, needs further exploration to understand the intricacies of the energy transfer mechanism between the Al plasmon and the TiO_2. It is evident from our measurements that the average photocatalytic reaction rate enhancement with Al plasmonics can be significant, and the plasmonic feature size strongly affects the enhancement.

Initial rates of MO decomposition were observed for 10 mins across all substrates, and MO concentration was determined via integration of the UV−vis MO absorption peak. MO decomposition over time was plotted and fitted to second-order polynomial functions. The first derivative of the fitted polynomial functions was calculated and plotted to analyze the rate (Figure 5B).[52] Negligible differences were observed between the rate of decomposition of MO between both larger (120 nm) Al features and blank TiO_2 thin-film control. The smaller (90 nm) Al features yielded a significant rate enhancement (0.022% decomposition/minute), and *an increase of ∼10x over the TiO_2control substrate is observed*. While it is a significant enhancement, the potential for further enhancement exists with refinement of plasmonic technology.

While a significant increase in the initial rate is observed in the smaller Al feature sizes compared to both the TiO_2 control and the larger Al feature sizes, it is short lived. The observed catalytic enhancement of the smaller Al feature sizes only exists for the first 7 mins of UV exposure. Also, it was noted that the COMSOL simulations showed significant plasmonic absorption peaks near the band edge of TiO_2, but these peaks were not observed in UV−vis measurements. This could be explained by inhomogeneities of the plasmonic-enhanced surface.

Al plasmonics tend to be altered in the presence of both hydroxyl radicals and broad-spectrum UV light.[53] Figure 6 displays UV−vis spectroscopic characterization of a deactivated (UV-exposed in MO solution) catalyst compared to active catalysts. While differences in absolute percentages are observed in the Al patterned TiO_2, line shape across reflectance, transmission, and absorption are nearly identical, indicating no distinct photophysical reason for catalyst deactivation. SEM imaging of catalysts after deactivation shows significant corrosion of the Al nanostructures (see supporting information), which likely causes the observed catalyst deactivation. It is believed that this deactivation pathway could be mitigated through a coating of the thin protective layer (e.g., Al_2O_3) over the Al nanostructures.[54,55]

Further study of the complex energy transfer between the active Al plasmons and the TiO_2 is a critical step in advancing not only this technology, but the interface of all fields employing plasmonics for energy transfer. Transferring this system from a patterned substrate-based system to a colloidal system can be a route towards increasing the applicability of this technology to industrial areas needing faster and improved water treatment technologies.

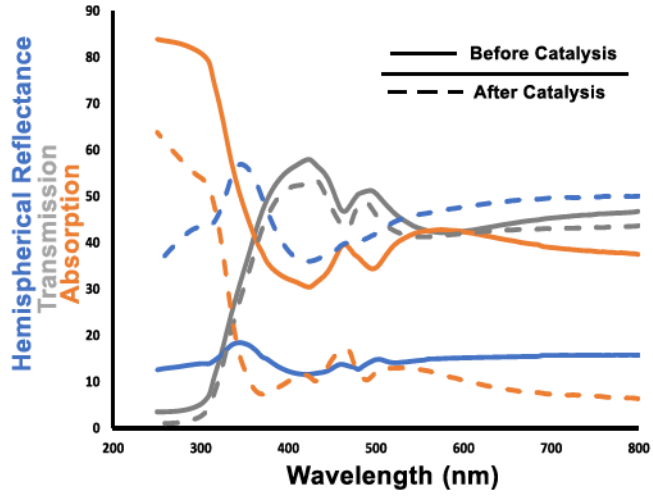

Figure 6. Uv−vis spectroscopic characterization of 90 nm plasmonic catalyst after reaction. Solid lines indicate measurements before catalysis, and dotted lines indicate those after catalysis (y-axis in %). Blue is measured hemispherical reflectance (R), gray is measured transmission (T), and orange is absorption (A) given by A = 100%- R -T.

CONCLUSIONS

Herein, we have successfully shown that aluminum UV plasmonic nanostructures closely tuned to the band gap of TiO_2, when placed on a surface constituting a catalytically active layer of TiO_2, can provide a significant rate enhancement (∼10×) of the photochemical decomposition of MO. While further work is needed to characterize the exact pathway of catalyst passivation and energy transfer, this is a step forward in developing methods for plasmonically enhancing UV-driven processes.

ASSOCIATED CONTENT

Supporting Information

The Supporting Information is available free of charge at https://pubs.acs.org/doi/10.1021/acs.jpcc.1c00613.

Detailed explanation of the kinetic methodology as well as the equations used for the graphical mapping, emission spectrum from the manufacturer of the lamp used, SEM images of catalysts before and after use, charts detailing average feature size and gap size, and raw UV−vis data of methyl orange (PDF)

AUTHOR INFORMATION

Corresponding Author

Allan S.P. Chang − *Materials Engineering Division, Lawrence Livermore National Lab, Livermore, California 94550, United States;* orcid.org/0000-0002-4893-5417; Email: chang43@llnl.gov

Authors

Ryan Brisbin − *Materials Engineering Division, Lawrence Livermore National Lab, Livermore, California 94550, United States; Department of Chemistry and Chemical*

Biology, School of Natural Sciences, University of California, Merced, California 95344, United States; orcid.org/0000-0003-0991-4629

Jenny Zhou − *Materials Engineering Division, Lawrence Livermore National Lab, Livermore, California 94550, United States*

Tiziana Bond − *Materials Engineering Division, Lawrence Livermore National Lab, Livermore, California 94550, United States;* orcid.org/0000-0002-4008-542X

Lars Voss − *Materials Engineering Division, Lawrence Livermore National Lab, Livermore, California 94550, United States*

Aaron J. Simon − *E-Program, Global Security Directorate, Lawrence Livermore National Lab, Livermore, California 94550, United States*

Ryan Baxter − *Department of Chemistry and Chemical Biology, School of Natural Sciences, University of California, Merced, California 95344, United States;* orcid.org/0000-0002-1341-5315

Complete contact information is available at: https://pubs.acs.org/10.1021/acs.jpcc.1c00613

Author Contributions

R.P.B. was responsible for kinetic experiments and analysis. J.Z. was responsible for catalyst synthesis and characterization. A.C. was responsible for COMSOL modeling, project creation, and guidance. T.B. was responsible for plasmonic and spectroscopy consultation. A.J.S. was responsible for water treatments and requirements consultation. L.V. was responsible for microfabrication and materials consultation. R.B. was responsible for chemical kinetics consultation.

Notes

The authors declare the following competing financial interest(s): A provisional patent was filed by Lawrence Livermore National Labs on behalf of the inventors under R/O 62/883,550.

■ ACKNOWLEDGMENTS

This work was performed under the auspices of the U.S. Department of Energy by Lawrence Livermore National Laboratory under Contract DE-AC52-07NA27344 and supported in part by the LDRD Program at LLNL under Grant 19-FS-015. This article is partly supported by the National Science Foundation under grant nos. NSF-CAREER 1752821.

■ REFERENCES

(1) Gong, R.; Ye, J.; Dai, W.; Yan, X.; Hu, J.; Hu, X.; Li, S.; Huang, H. Adsorptive Removal of Methyl Orange and Methylene Blue from Aqueous Solution with Finger-Citron-Residue-Based Activated Carbon. *Ind. Eng. Chem. Res.* **2013**, *52*, 14297−14303.

(2) Crini, G. Non-Conventional Low-Cost Adsorbents for Dye Removal: A Review. *Bioresour. Technol.* **2006**, *97*, 1061−1085.

(3) Hou, W.; Liu, Z.; Pavaskar, P.; Hung, W. H.; Cronin, S. B. Plasmonic Enhancement of Photocatalytic Decomposition of Methyl Orange under Visible Light. *J. Catal.* **2011**, *277*, 149−153.

(4) Banat, I. M.; Nigam, P.; Singh, D.; Marchant, R. Microbial Decolorization of Textile-Dye-Containing Effluents: A Review. *Bioresour. Technol.* **1996**, *58*, 217−227.

(5) Nakata, K.; Fujishima, A. TiO 2 Photocatalysis: Design and Applications. *J. Photochem. Photobiol. C Photochem. Rev.* **2012**, *13*, 169−189.

(6) Paramasivam, I.; Jha, H.; Liu, N.; Schmuki, P. A Review of Photocatalysis Using Self-Organized TiO 2 Nanotubes and Other Ordered Oxide Nanostructures. *Small* **2012**, *8*, 3073−3103.

(7) Finegold, L.; Cude, J. L. Electrochemical Photolysis of Water at a Semiconductor Electrode. *Nature* **1972**, *238*, 38−40.

(8) Fujishima, A.; Zhang, X.; Tryk, D. TiO2 Photocatalysis and Related Surface Phenomena. *Surf. Sci. Rep.* **2008**, *63*, 515−582.

(9) Fujishima, A.; Rao, T. N.; Tryk, D. A. TiO2 Photocatalysts and Diamond Electrodes. *Electrochim. Acta* **2000**, *45*, 4683−4690.

(10) Su, L.; Tong, P.; Zhang, L.; Luo, Z.; Fu, C.; Tang, D.; Zhang, Y. Photoelectrochemical Immunoassay of Aflatoxin B 1 in Foodstuff Based on Amorphous TiO 2 and CsPbBr 3 Perovskite Nanocrystals. *Analyst* **2019**, *144*, 4880−4886.

(11) Shu, J.; Qiu, Z.; Lv, S.; Zhang, K.; Tang, D. Plasmonic Enhancement Coupling with Defect-Engineered TiO2-x: A Mode for Sensitive Photoelectrochemical Biosensing. *Anal. Chem.* **2018**, *90*, 2425−2429.

(12) Cai, G.; Yu, Z.; Tang, D. Actuating Photoelectrochemical Sensing Sensitivity Coupling Core-Core-Shell Fe3O4@C@TiO2 with Molecularly Imprinted Polypyrrole. *Talanta* **2020**, *219*, No. 121341.

(13) Cai, G.; Yu, Z.; Ren, R.; Tang, D. Exciton−Plasmon Interaction between AuNPs/Graphene Nanohybrids and CdS Quantum Dots/TiO 2 for Photoelectrochemical Aptasensing of Prostate-Specific Antigen. *ACS Sensors* **2018**, *3*, 632−639.

(14) Brezová, V.; Jankovičová, M.; Soldán, M.; Blažková, A.; Reháková, M.; Šurina, I.; Čeppan, M.; Havlínová, B. Photocatalytic Degradation of P-Toluenesulphonic Acid in Aqueous Systems Containing Powdered and Immobilized Titanium Dioxide. *J. Photochem. Photobiol., A* **1994**, *83*, 69−75.

(15) Matthews, R. W. Kinetics of Photocatalytic Oxidation of Organic Solutes over Titanium Dioxide. *J. Catal.* **1988**, *111*, 264−272.

(16) Faust, B. C.; Hoffmann, M. R. Photoinduced Reductive Dissolution of α-Fe2O3 by Bisulfite. *Environ. Sci. Technol.* **1986**, *20*, 943−948.

(17) Rosenberg, I.; Brock, J. R.; Heller, A. Collection Optics of TiO2 Photocatalyst on Hollow Glass Microbeads Floating on Oil Slicks. *J. Phys. Chem.* **1992**, *96*, 3423−3428.

(18) Gomes da Silva, C.; Faria, J. L. Photochemical and Photocatalytic Degradation of an Azo Dye in Aqueous Solution by UV Irradiation. *J. Photochem. Photobiol., A* **2003**, *155*, 133−143.

(19) Lee, S. Y.; Park, S. J. TiO2 Photocatalyst for Water Treatment Applications. *J. Ind. Eng. Chem.* **2013**, *19*, 1761−1769.

(20) Dai, K.; Chen, H.; Peng, T.; Ke, D.; Yi, H. Photocatalytic Degradation of Methyl Orange in Aqueous Suspension of Mesoporous Titania Nanoparticles. *Chemosphere* **2007**, *69*, 1361−1367.

(21) Liu, S.; Yang, J. H.; Choy, J. H. Microporous SiO2-TiO2 Nanosols Pillared Montmorillonite for Photocatalytic Decomposition of Methyl Orange. *J. Photochem. Photobiol., A* **2006**, *179*, 75−80.

(22) Liao, D. L.; Badour, C. A.; Liao, B. Q. Preparation of Nanosized TiO2/ZnO Composite Catalyst and Its Photocatalytic Activity for Degradation of Methyl Orange. *J. Photochem. Photobiol., A* **2008**, *194*, 11−19.

(23) Wang, J.; Guo, B.; Zhang, X.; Zhang, Z.; Han, J.; Wu, J. Sonocatalytic Degradation of Methyl Orange in the Presence of TiO 2 Catalysts and Catalytic Activity Comparison of Rutile and Anatase. *Ultrason. Sonochem.* **2005**, *12*, 331−337.

(24) Tong, T.; Zhang, J.; Tian, B.; Chen, F.; He, D. Preparation of Fe3+-Doped TiO2 Catalysts by Controlled Hydrolysis of Titanium Alkoxide and Study on Their Photocatalytic Activity for Methyl Orange Degradation. *J. Hazard. Mater.* **2008**, *155*, 572−579.

(25) Wang, X. H.; Li, J. G.; Kamiyama, H.; Moriyoshi, Y.; Ishigaki, T. Wavelength-Sensitive Photocatalytic Degradation of Methyl Orange in Aqueous Suspension over Iron(III)-Doped TiO2 Nanopowders under UV and Visible Light Irradiation. *J. Phys. Chem. B* **2006**, *110*, 6804−6809.

(26) Tasaki, T.; Wada, T.; Fujimoto, K.; Kai, S.; Ohe, K.; Oshima, T.; Baba, Y.; Kukizaki, M. Degradation of Methyl Orange Using

Short-Wavelength UV Irradiation with Oxygen Microbubbles. *J. Hazard. Mater.* **2009**, *162*, 1103−1110.
(27) Vinodgopal, K.; Kamat, P. V. Enhanced Rates of Photocatalytic Degradation of an Azo Dye Using SnO2/TiO2 Coupled Semiconductor Thin Films. *Environ. Sci. Technol.* **1995**, *29*, 841−845.
(28) Li, Y.; Li, X.; Li, J.; Yin, J. Photocatalytic Degradation of Methyl Orange by TiO2-Coated Activated Carbon and Kinetic Study. *Water Res.* **2006**, *40*, 1119−1126.
(29) Prado, A. G. S.; Costa, L. L. Photocatalytic Decouloration of Malachite Green Dye by Application of TiO2 Nanotubes. *J. Hazard. Mater.* **2009**, *169*, 297−301.
(30) Guo, W.; Zhang, F.; Lin, C.; Wang, Z. L. Direct Growth of TiO2 Nanosheet Arrays on Carbon Fibers for Highly Efficient Photocatalytic Degradation of Methyl Orange. *Adv. Mater.* **2012**, *24*, 4761−4764.
(31) Nie, J.; Patrocinio, A. O. T.; Hamid, S.; Sieland, F.; Sann, J.; Xia, S.; Bahnemann, D. W.; Schneider, J. New Insights into the Plasmonic Enhancement for Photocatalytic H2 Production by Cu-TiO2 upon Visible Light Illumination. *Phys. Chem. Chem. Phys.* **2018**, *20*, 5264−5273.
(32) Jani, N. A.; Haw, C. Y.; Chiu, W. S.; Rahman, S. A.; Lim, Y. C.; Khiew, P. S.; Yaghoubi, A. Understanding the Effect of Plasmonic Enhancement on Photocatalytic Activity of TiO2 Nanotube Arrays. *Mater. Charact.* **2017**, *128*, 134−141.
(33) Zhang, H.; Chen, Y.; Wang, H.; Hu, S.; Xia, K.; Xiong, X.; Huang, W.; Lu, H.; Yu, J.; Guan, H.; He, M.; Liu, W.; Zhang, J.; Luo, Y.; Xie, Z.; Chen, Z. Titanium Dioxide Nanoparticle Modified Plasmonic Interface for Enhanced Refractometric and Biomolecular Sensing. *Opt. Express* **2018**, *26*, No. 33226.
(34) Asapu, R.; Claes, N.; Ciocarlan, R. G.; Minjauw, M.; Detavernier, C.; Cool, P.; Bals, S.; Verbruggen, S. W. Electron Transfer and Near-Field Mechanisms in Plasmonic Gold-Nanoparticle-Modified TiO2 Photocatalytic Systems. *ACS Appl. Nano Mater.* **2019**, *2*, 4067−4074.
(35) Khatun, F.; Abd Aziz, A.; Sim, L. C.; Monir, M. U. Plasmonic Enhanced Au Decorated TiO2 Nanotube Arrays as a Visible Light Active Catalyst towards Photocatalytic CO2 Conversion to CH4. *J. Environ. Chem. Eng.* **2019**, *7*, No. 103233.
(36) Hao, Q.; Wang, C.; Huang, H.; Li, W.; Du, D.; Han, D.; Qiu, T.; Chu, P. K. Aluminum Plasmonic Photocatalysis. *Sci. Rep.* **2015**, *5*, 1−7.
(37) Honda, M.; Kumamoto, Y.; Taguchi, A.; Saito, Y.; Kawata, S. Efficient UV Photocatalysis Assisted by Densely Distributed Aluminum Nanoparticles. *J. Phys. D: Appl. Phys.* **2015**, *48*, No. 184006.
(38) Taherniya, A.; Raoufi, D. The Annealing Temperature Dependence of Anatase TiO2 Thin Films Prepared by the Electron-Beam Evaporation Method. *Semicond. Sci. Technol.* **2016**, *31*, No. 125012.
(39) Bakri, A. S.; Sahdan, M. Z.; Adriyanto, F.; Raship, N. A.; Said, N. D. M.; Abdullah, S. A.; Rahim, M. S. *Effect of Annealing Temperature of Titanium Dioxide Thin Films on Structural and Electrical Properties*. AIP Conf. Proc. 2017, *1788*.
(40) Cheung, C. L.; Nikolić, R. J.; Reinhardt, C. E.; Wang, T. F. Fabrication of Nanopillars by Nanosphere Lithography. *Nanotechnology* **2006**, *17*, 1339−1343.
(41) Chen, J.; Dong, P.; Di, D.; Wang, C.; Wang, H.; Wang, J.; Wu, X. Controllable Fabrication of 2D Colloidal-Crystal Films with Polystyrene Nanospheres of Various Diameters by Spin-Coating. *Appl. Surf. Sci.* **2013**, *270*, 6−15.
(42) Linsebigler, A. L.; Lu, G.; Yates, J. T., Jr. Photocatalysis on TiO2 Surfaces: Principles, Mechanisms, and Selected Results. *Chem. Rev.* **1995**, *95*, 735−758.
(43) Hulteen, J. C.; van Duyne, R. P. Nanosphere Lithography: A Materials General Fabrication Process for Periodic Particle Array Surfaces. *J. Vac. Sci. Technol. A Vac., Surf. Film.* **1995**, *13*, 1553−1558.
(44) Wang, Q. D.; Ye, L.; Wang, L.; Li, P. Y.; Cao, Y.; Li, Y. Rapid Nanopatterning Technique Based on Monolayer Silica Nanosphere Close-Packing by Spin Coating. *Sci. China Technol. Sci.* **2016**, *59*, 1573−1580.
(45) Zhang, C.; Cvetanovic, S.; Pearce, J. M. Fabricating Ordered 2-D Nano-Structured Arrays Using Nanosphere Lithography. *MethodsX* **2017**, *4*, 229−242.
(46) Scholes, G. D. Long-Range Resonance Energy Transfer in Molecular Systems. *Annu. Rev. Phys. Chem.* **2003**, *54*, 57−87.
(47) Ma, X. C.; Dai, Y.; Yu, L.; Huang, B. B. Energy Transfer in Plasmonic Photocatalytic Composites. *Light Sci. Appl.* **2016**, *5*, No. e16017.
(48) Cushing, S. K.; Li, J.; Meng, F.; Senty, T. R.; Suri, S.; Zhi, M.; Li, M.; Bristow, A. D.; Wu, N. Photocatalytic Activity Enhanced by Plasmonic Resonant Energy Transfer from Metal to Semiconductor. *J. Am. Chem. Soc.* **2012**, *134*, 15033−15041.
(49) Gellé, A.; Jin, T.; de la Garza, L.; Price, G. D.; Besteiro, L. V.; Moores, A. Applications of Plasmon-Enhanced Nanocatalysis to Organic Transformations. *Chem. Rev.* **2020**, *120*, 986−1041.
(50) Luo, Q.; Zhang, C.; Deng, X.; Zhu, H.; Li, Z.; Wang, Z.; Chen, X.; Huang, S. Plasmonic Effects of Metallic Nanoparticles on Enhancing Performance of Perovskite Solar Cells. *ACS Appl. Mater. Interfaces* **2017**, *9*, 34821−34832.
(51) Schuller, J. A.; Barnard, E. S.; Cai, W.; Jun, Y. C.; White, J. S.; Brongersma, M. L. Plasmonics for Extreme Light Concentration and Manipulation. *Nat. Mater.* **2010**, *9*, 193−204.
(52) Blackmond, D. G. Reaction Progress Kinetic Analysis: A Powerful Methodology for Mechanistic Studies of Complex Catalytic Reactions. *Angew. Chem., Int. Ed.* **2005**, *44*, 4302−4320.
(53) Barulin, A.; Claude, J. B.; Patra, S.; Moreau, A.; Lumeau, J.; Wenger, J. Preventing Aluminum Photocorrosion for Ultraviolet Plasmonics. *J. Phys. Chem. Lett.* **2019**, *10*, 5700−5707.
(54) Gutierrez, Y.; Ortiz, D.; Sanz, J. M.; Saiz, J. M.; Gonzalez, F.; Everitt, H. O.; Moreno, F. How an Oxide Shell Affectsthe Ultraviolet Plasmonic Behavior of Ga, Mg, and Al Nanostructures. *Opt. Express* **2016**, *24*, 20621−20631.
(55) Wang, J.; Wu, Z.; Wei, J.; Hu, J.; Yu, H.; Su, G.; Hu, L.; Yan, X.; Zhan, P.; Liu, F. Improving Aluminum Ultraviolet Plasmonic Activity Through a 1 nm ta-C Film. *ACS Appl. Mater. Interfaces* **2021**, *13*, 7672−7679.

https://doi.org/10.1021/acs.jpcc.1c00613
J. Phys. Chem. C 2021, 125, 9730−9735